

Origins of ultra–diffuse galaxies in the Coma cluster – II. Constraints from their stellar populations

Anna Ferré-Mateu¹★, Adebisola Alabi², Duncan A. Forbes¹, Aaron J. Romanowsky^{3,2},
Jean Brodie², Viraj Pandya², Ignacio Martín-Navarro², Sabine Bellstedt¹,
Asher Wasserman², Maria Stone³ and Nobuhiro Okabe^{4,5,6}

¹ Centre for Astrophysics & Supercomputing, Swinburne University of Technology, Hawthorn VIC 3122, Australia

² University of California Observatories, 1156 High St., Santa Cruz, CA 95064, USA

³ Department of Physics and Astronomy, San José State University, San Jose, CA 95192, USA

⁴ Department of Physical Science, Hiroshima University, 1-3-1, Kagamiyama, Higashi-Hiroshima, Hiroshima 739-8526, Japan

⁵ Hiroshima Astrophysical Science Center, Hiroshima University, 1-3-1, Kagamiyama, Higashi-Hiroshima, Hiroshima 739-8526, Japan

⁶ Core Research for Energetic Universe, Hiroshima University, 1-3-1, Kagamiyama, Higashi-Hiroshima, Hiroshima 739-8526, Japan

Submitted to MNRAS

ABSTRACT

In this second paper of the series we study, with new Keck/DEIMOS spectra, the stellar populations of 7 spectroscopically confirmed ultra–diffuse galaxies (UDGs) in the Coma cluster. We find typically intermediate to old ages (~ 7 Gyr), low metallicities ($[Z/H] \sim -0.7$ dex) and slightly super-solar abundance patterns ($[Mg/Fe] \sim +0.16$ dex). These properties are similar to those of dwarf galaxies inhabiting the same area in the cluster and are mostly consistent with being the continuity of the stellar mass scaling relations of more massive galaxies. These UDGs’ star formation histories imply a relatively recent infall into the Coma cluster, consistent with the theoretical predictions for a dwarf–like origin. However, considering the scatter in the resulting properties and including other UDGs in Coma, together with the results from the velocity phase–space study of the Paper I in this series, a mixed-bag of origins is needed to explain the nature of all UDGs. Our results thus reinforce a scenario in which most of the UDGs are field dwarf galaxies that become quenched through their later infall in cluster environments, whereas some other UDGs are genuine primordial galaxies that failed to develop due to an early quenching phase. The unknown proportion of dwarf–like to primordial–like UDGs leaves the enigma of the nature of UDGs still open.

Key words: galaxies – galaxies: evolution – galaxies: formation – galaxies: kinematics and dynamics – galaxies: stellar content – galaxies: dwarfs

1 INTRODUCTION

Although low-surface brightness galaxies were discovered many decades ago (e.g. Impey, Bothun & Malin 1988; Dalcanton et al. 1997), the recent finding of a large number of them in the Coma cluster (e.g. van Dokkum et al. 2015a) has refuelled the interest by the scientific community for this intriguing class of galaxies. Relabelled as ultra–diffuse galaxies (UDGs), they have been reported to exist across a wide range of environments. Large numbers of them have been reported in clusters (e.g. Koda et al. 2015; Muñoz et al. 2015; Mihos et al. 2015; Beasley et al. 2016; Beasley & Trujillo 2016; Yagi et al. 2016; van der Burg, Muzzin & Hoekstra 2016; Román & Trujillo 2017a; Janssens et al. 2017;

Lee et al. 2017; Venhola et al. 2017), but others have been also found in groups (e.g. Makarov et al. 2015; Merritt et al. 2016; Román & Trujillo 2017b; Trujillo et al. 2017; van der Burg et al. 2017, Shi et al. 2017) and occasionally in the field (e.g. Martínez-Delgado et al. 2016; Bellazzini et al. 2017; Leisman et al. 2017). UDGs share similar luminosities and stellar masses to dwarfs ($L_V \sim 10^8 L_\odot$; $M_* \sim 10^7$ – $10^8 M_\odot$), but are as large as ellipticals ($R_e \sim 1.5$ – 4.6 kpc) with typically spheroidal shapes (Burkert 2017), and some of them have been found to contain large amounts of dark matter (e.g. Beasley & Trujillo 2016; van Dokkum et al. 2016). With their origin still unknown, it is not clear what role they play in the wider paradigm of galaxy evolution.

A myriad of studies have suggested various pathways for the formation of UDGs. One such pathway is that they are

★ E-mail: aferremateu@swin.edu.au (AFM)

‘failed’ galaxies (e.g. van Dokkum et al. 2015b; Peng & Lim 2016; van Dokkum et al. 2016). Under this scenario, the assumption is that the star formation of the primordial halo was truncated at very early epochs ($z > 2$), most likely produced by the infall of such undeveloped halos into the cluster environment (Yozin & Bekki 2015). This would thus explain the UDG formation in high density environments. However, it fails to explain the presence of UDGs in lower densities or even in isolation. Therefore, UDGs have also been proposed to simply be dwarf-like galaxies that either live in high-spin halos that prevent objects becoming more condensed (Amorisco & Loeb 2016; Rong et al. 2017) or that are formed through internal processes, i.e. outflow-driven gas feedback that disperses the matter, creating a diffuse galaxy (e.g. Chan et al. 2017; Di Cintio et al. 2017). Such dwarf-like scenarios predict the presence of UDGs in isolated environments, allowing for the presence of gas in such galaxies (e.g. Jones et al. 2017, Leisman et al. 2017; Papastergis, Adams & Romanowsky 2017). Therefore, in the normal-dwarf scenarios, UDGs would be created in dwarf-sized halos in the field that are later accreted into groups and clusters, where physical processes such as ram-pressure stripping and starvation become more prominent, removing the gas reservoir and quenching the star formation in the UDG. This idea is motivated by the finding that red spheroidal UDGs typically populate galaxy clusters, whereas bluer, irregularly shaped ones, are more commonly found in groups and in isolation (e.g. Román & Trujillo 2017b).

Interestingly, there are both evidence and theoretical predictions supporting the competing scenarios, which suggest that the true nature of UDGs might not follow a unique formation pathway, but have a mixed-bag of origins.

There is one key diagnostic to understand the origins of UDGs that has remained quite elusive to date – the study of their stellar populations. By comparing such properties to those expected from the diverse formation scenarios one should be able to differentiate between the possible origins. For example, under the ‘failed’ galaxy scenario where the primordial halos were quenched at very early times, one would expect stellar populations with very old ages and high mean $[\text{Mg}/\text{Fe}]$ ratios related to the fast formation timescales, e.g. Yozin & Bekki (2015). In contrast, favouring a normal dwarf galaxy interpretation, Rong et al. (2017) predicted from their cosmological simulations that UDGs formed late in halos of high spin, with extended star formation histories and a mean age of 7 Gyr for UDGs (some 2.5 Gyr younger than the typical dwarf galaxy in their simulation). Similarly, analysing UDGs with high levels of feedback but normal spin parameters within the FIRE simulation, Chan et al. (2017) suggested that UDGs have a range of a quenching timescales and hence predicted a broad range of UDG ages, i.e. 2–12 Gyr.

Observationally, the majority of studies have addressed the issue of UDG stellar populations from a photometric point of view (e.g. Pandya et al. 2017, hereafter P+17; Román & Trujillo 2017a; Trujillo et al. 2017) or by studying their globular cluster properties (e.g. Beasley et al. 2016, hereafter BeasleyT2016; Peng & Lim 2016; van Dokkum et al. 2017). Owing to the low surface brightness and extended size of UDGs, spectroscopy is very challenging and time-consuming, but crucial for revealing the formation histories of these objects. To date, only a couple of studies have

attempted such a task. Kadowaki, Zaritsky & Donnerstein (2017) obtained spectra of 4 Coma UDGs using the Large Binocular Telescope. However, due to the low signal-to-noise (S/N) of their spectra they had to stack them into one single spectrum, which was then visually compared to stellar population models. They concluded that their Coma UDGs were most compatible with being old and very metal-poor ($[\text{Fe}/\text{H}] < -1.5$). By combining many fibres on the Apache Point Observatory telescope and a long integration time, Gu et al. (2017) hereafter P+17 were able to analyse individual spectra of 3 other Coma UDGs. From a spectral and photometric analysis, they concluded that all three galaxies were old (~ 9 Gyr) and relatively metal-poor ($[\text{Fe}/\text{H}] \sim -1$).

Here we extend the characterisation of high density environment UDGs by presenting the stellar populations of 7 additional UDGs that have been spectroscopically confirmed as Coma cluster members from new Keck/DEIMOS spectra. We combine this with literature data to examine the distributions of age, metallicity and α -element overabundance for Coma cluster UDGs, and to see how they compare to the properties of other galaxies in Coma. With the additional information revealed by the star formation histories (SFHs) of our UDGs, we discuss the implications for their formation mechanisms and possible origin(s).

Section 2 presents a summary of the new Keck/DEIMOS data, the sample, the observations and the data reduction, although the reader is encouraged to read the first manuscript of the series (Alabi et al. 2018, submitted; Paper I hereafter) for a full description. Section 3 describes the stellar population analysis performed and we discuss the possible origins for the Coma UDGs in section 4. We assume a Λ CDM cosmology with $H_0 = 70 \text{ km s}^{-1} \text{ Mpc}^{-1}$, $\Omega_m = 0.27$ and $\Omega_\Lambda = 0.73$ to allow for direct comparisons with the theoretical predictions and literature data, with an adopted distance for Coma of $D_L = 100 \text{ Mpc}$.

2 DATA

2.1 Sample selection

A detailed description of the selected candidates and DEIMOS mask production can be found in Paper I, but we summarise here the most relevant points of the sample selection. Candidate UDGs were selected from the catalog of Yagi et al. (2016), based on deep Subaru/Suprime-Cam imaging of the Coma cluster (Okabe et al. 2014). Using criteria that included half-light radii of $R_e > 0.7 \text{ kpc}$ (a factor of 2 smaller than Dragonfly UDGs of van Dokkum et al. 2015a), total magnitude $-17 < M_R < -9$, and a mean surface brightness within $1R_e$ of $24 < \mu_R < 27 \text{ mag arcsec}^{-2}$, they identified 854 Coma cluster candidate UDGs. In order to target as many UDGs as possible we focused on a $16 \times 4 \text{ sq. arcmin}$ region (i.e. the footprint of a DEIMOS mask) at approximately 0.2° ($\sim 340 \text{ kpc}$) south of the centre of the Coma cluster (see Fig 3 of Paper I for reference). This mask, which is shown in Figure 1 and which we call ‘central’ compared to the more external one from Paper I, contained a total of 50 slits – half of them targeting UDGs. The rest of slits were filled with galaxies of different types but typically higher surface brightnesses than the UDGs in the study. We thus make a luminosity cut to separate between galaxies

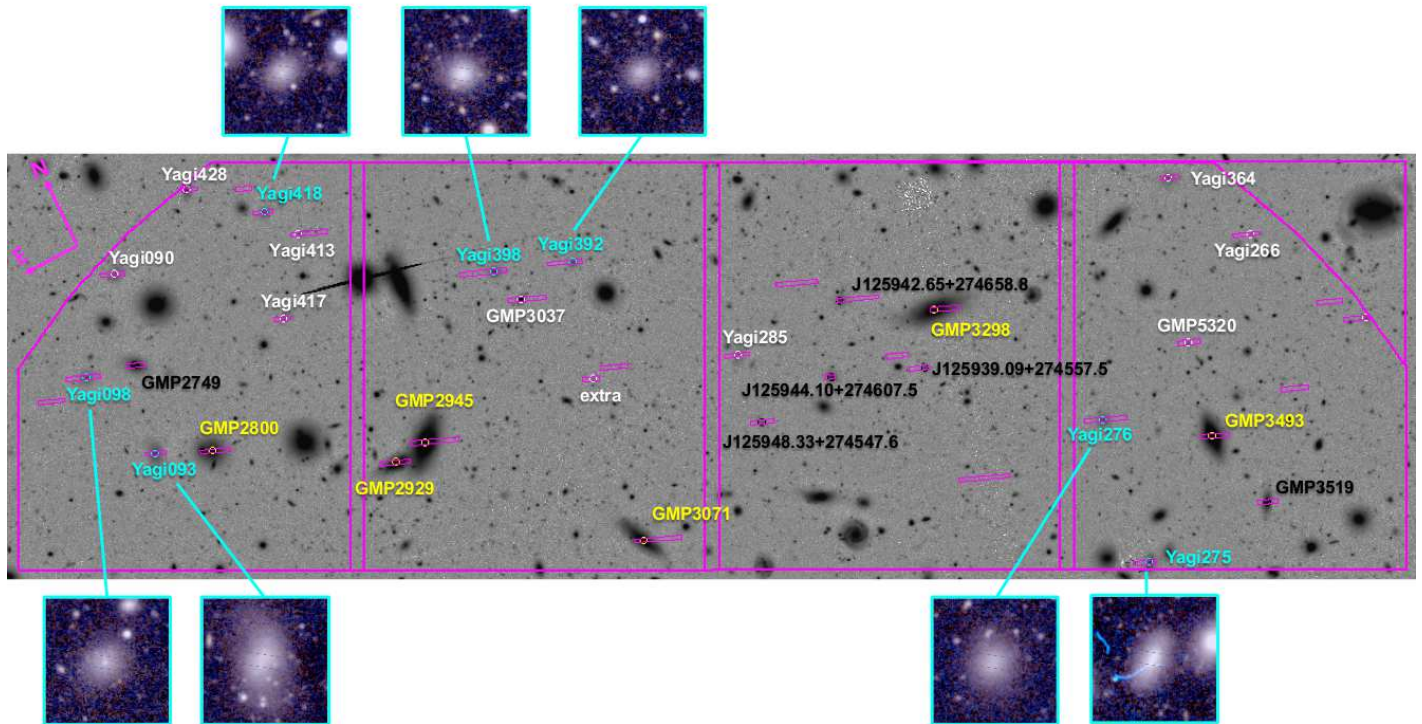


Figure 1. ‘Central’ DEIMOS Coma mask: Coma Cluster V-band Subaru/Suprime-Cam image (Okabe et al. 2014) with the layout of the central DEIMOS mask (pink) shown. The mask covers roughly 16×4 sq. arcmin ($\sim 450 \times 110$ kpc at the Coma distance) and is located at approximately 0.2° south of the centre of the Coma Cluster, with an angle of 160° (see Fig. 3 of Paper I). The cyan labelled galaxies correspond to the UDGs analysed in this work, whereas the yellow are high-luminosity galaxies and the black are low-luminosity ones, both used as control samples. The white labelled galaxies are the remaining galaxies that did not have enough S/N for a stellar population analysis but whose recession velocities are derived in Paper I. Unlabelled slits correspond to sky slits or alignment stars. The seven UDGs studied in this work are also shown in $30 \times 30''$ thumbnails combining V and R_c images.

that are dwarf-like and those more luminous galaxies, which are mostly spiral-like. Therefore we will use the following nomenclature throughout the paper: high-luminosity galaxies (HLG; $R > 17$) that are typically late-type galaxies, and low-luminosity galaxies (LLG; $R > 17$) which are typically dwarf galaxies.

2.2 Observations and data reduction

Observations were carried out using the DEIMOS instrument on the Keck II telescope. Over 3 nights in 2017 (April 27–29) we obtained a total of 29 individual exposures of 30 min each, giving a total on source exposure time of 14.5 hr for this central Coma mask, with seeing conditions of 0.6 – $0.8''$ and generally clear skies. We used the 600 lines mm^{-1} grating centred at 6000\AA , which delivers a wavelength coverage spanning ~ 4300 – 9600\AA depending on the position of the slit. Each slit was opened $3''$ to match to the typical size of Coma UDGs. However, this configuration was too coarse to measure internal velocity dispersions, as it results in a FWHM resolution of $\sim 14\text{\AA}$ (or $\sigma \sim 300 \text{ km s}^{-1}$ at the central wavelength).

The raw data were reduced using the `spec2D` pipeline (Cooper et al. 2012). As we are dealing with faint sources, we experimented with different object definition and sky-subtraction approaches but ultimately adopted the default

procedure of the `spec2D` pipeline as preferred. The output 1D spectra were sky-subtracted and wavelength calibrated. We also applied a relative flux calibration that corrects for the spectral shape using a set of standard stars that were also observed with the same setup. Paper I presents the analysis of the recession velocities of the galaxies in the mask, confirming them as Coma members. We thus used those published values to shift the spectra to the rest frame before performing any stellar population analysis. Because the instrumental dispersion already matched the stellar population models used in Section 3, there was no need to further broaden our spectra.

Although the central mask contained 15 slits targeting candidate UDGs, only 7 of them had sufficient signal-to-noise ($S/N > 15$; see Cid Fernandes et al. 2014) for a tentative stellar population analysis. In Table 1 we list the coordinates, recession velocities (as derived in Paper I), R -band magnitudes, colours, and effective radii from Yagi et al. (2016) for the 7 UDGs. Two of them are found in common with the van Dokkum et al. (2015a) Dragonfly catalog: Yagi 093=DF26 and Yagi 276=DF28. Interestingly, only one of the seven UDGs (Yagi 093) shows some indications of being disrupted, which is in agreement with the general lack of tidal features in UDGs in the central parts of Coma (e.g. Mowla et al. 2017). Yagi 398 is on the limit of the UDG size criteria defined by van Dokkum et al. (2015a) (with

Galaxy	Type	R.A. (J2000)	Dec. (J2000)	Vr (km s ⁻¹)	R (mag)	B-R (mag)	Re (kpc)
Yagi 093 (DF26)	UDG	13:00:20.614	+27:47:12.31	6611±137	18.9	0.96	3.49
Yagi 098	UDG	13:00:23.201	+27:48:17.14	5980±82	19.6	0.96	2.30
Yagi 275	UDG	12:59:29.891	+27:43:03.07	4847±149	19.2	0.92	2.93
Yagi 276 (DF28)	UDG	12:59:30.463	+27:44:50.40	7343±102	19.6	0.90	2.25
Yagi 392	UDG	12:59:56.174	+27:48:12.78	7748±161	20.7	0.97	1.46
Yagi 398	UDG	13:00:00.414	+27:48:19.68	4180±167	20.1	0.96	1.34
Yagi 418	UDG	13:00:11.710	+27:49:40.99	8335±187	20.4	0.93	1.57
J125944.10+274607.5	LLG (dE)	12:59:44.105	+27:46:07.57	6109±127	19.2	–	0.92
J125942.65+274658.8	LLG (dE)	12:59:42.650	+27:46:59.44	5418±163	20.2	–	1.36
J125948.33+274547.6	LLG (dE)	12:59:48.372	+27:45:48.21	8039±109	21.2	–	1.37
J125939.09+274557.5	LLG (dE)	12:59:39.096	+27:45:57.53	7791±164	20.1	–	0.88
GMP 2749	LLG (dE)	13:00:20.482	+27:48:17.03	5846±74	18.4	–	1.59
GMP 3519	LLG (S)	12:59:22.944	+27:43:24.48	4062±167	18.7	–	1.88
GMP 2800	HLG (dE0)	13:00:17.553	+27:47:03.94	7001±132	16.7	–	2.92
GMP 2923	HLG (SBb)	13:00:08.054	+27:46:24.08	8652±125	16.8	–	2.09
GMP 2945	HLG (Sa)	13:00:06.288	+27:46:32.88	6091±66	14.6	–	2.63
GMP 3071	HLG (Sb)	12:59:56.112	+27:44:46.72	8810±99	16.2	–	1.39
GMP 3298	HLG (S0/a)	12:59:37.828	+27:46:36.62	5554±41	15.3	–	4.27
GMP 3493	HLG (Sa)	12:59:24.931	+27:44:19.86	6001±80	14.9	–	1.38

Table 1. Ultra-diffuse galaxy sample and other Coma cluster targets. Summary of the observational and main properties of the UDGs and control sample galaxies studied in this work. For the 7 UDGs we use the ID from Yagi et al. (2016) and quote if they also have a Dragonfly name (van Dokkum et al. 2015a). For the rest of control galaxies, separated by between , we use their most common name as identified in the SDSS. The galaxy type is also shown, as quoted in either SIMBAD or NED, with their corresponding coordinates. The quoted recession velocities, R -band magnitudes, the $B - R$ colours and effective radii are as quoted in Paper I (from Yagi et al. (2016) for the UDGs and SDSS/SIMBAD/NED for the control galaxies). We separate between LLG and HLG at $R=17$.

$R_e=1.3$ kpc) but is within the limits from Yagi et al. (2016) and those allowed in the theoretical simulations. Therefore we keep this galaxy in the UDG class, although we will check if our results in Section 4 are affected by such assumption.

The additional galaxies included in the mask that have sufficient S/N are also described in Table 1. Four LLGs are newly confirmed Coma dwarf galaxies, one of them, J125942.65+274658.8 with properties that resemble more to UDGs than dwarfs. Like with Yagi 398, we keep this object in the original classification but check for inconsistencies in the results. Two other filler objects (GMP 2800 and GMP 3298) are found in common with the sample of Coma red dwarf galaxies from Smith et al. (2009) (hereafter S+09), for which we find consistent age and metallicity values (see following sections).

In Figure 2 we show the spectra of the 7 UDGs in this work, corresponding to the best spectral range used for the stellar population analysis in Section 3, which is virtually free of sky residual and instrument flexures that were not properly corrected during the reduction process. This spectral range is sufficient to perform the stellar population analysis as it encompasses the most relevant features needed for it, which are highlighted by the dotted vertical lines. Note that both the spectra and the fit shown have been normalised for illustration purposes.

3 STELLAR POPULATION ANALYSIS

For the stellar population analysis we employ the newest extension of the MILES SSPs (Single-Stellar Population models; Vazdekis et al. 2016), which covers a wide range of ages, metallicities and initial mass functions. It has been

shown that at low stellar masses and low velocity dispersions such as those of the objects studied here, the impact of a varying initial mass function is very mild (e.g. Ferré-Mateu, Vazdekis & de la Rosa 2013), therefore we assume a universal Kroupa IMF to directly compare with literature results. In the following, we study the stellar population properties with a two-fold approach, using the best spectral range of our data (4700–5400 Å, see Fig. 2), which is virtually free from sky residuals, bad pixels and instrument flexure.

We first perform a line-index analysis, using the age-sensitive indices $H\beta$ and $H\beta_0$ compared to a set of metallicity indicators (Fe5015, Fe5270, Fe5335, Mgb, and also the composite indices $\langle Fe \rangle'$, [MgFe50] and [MgFe]′). This provides a set of luminosity-weighted ages, [Fe/H] metallicities, [Z/H] total metallicities and α -abundances. However, because our spectral range only contains the α -element Mg, we use the [Mg/Fe] abundances as the $[\alpha/Fe]$ one (see Appendix for a full description on the line-indices used). We also use the full spectral fitting approach, which creates a combination of SSP model predictions that best matches each spectrum. This provides not only mean luminosity-weighted values but also mass-weighted ones and the SFHs of the galaxies over time, i.e. the amount of stellar mass/light that was created over cosmic time.

For the full spectral fitting exercise we use two different codes: one for the relative-flux calibrated spectra (STARLIGHT; Cid Fernandes et al. 2005) and another applicable to non-flux calibrated spectra (STECKMAP; Ocavirk et al. 2006). Despite providing similar results on terms of mean quantities, each code delivers the SFH in a different way, i.e. STARLIGHT tends to produce SFHs that are more bursty-like whereas STECKMAP normalises the result so it provides a more

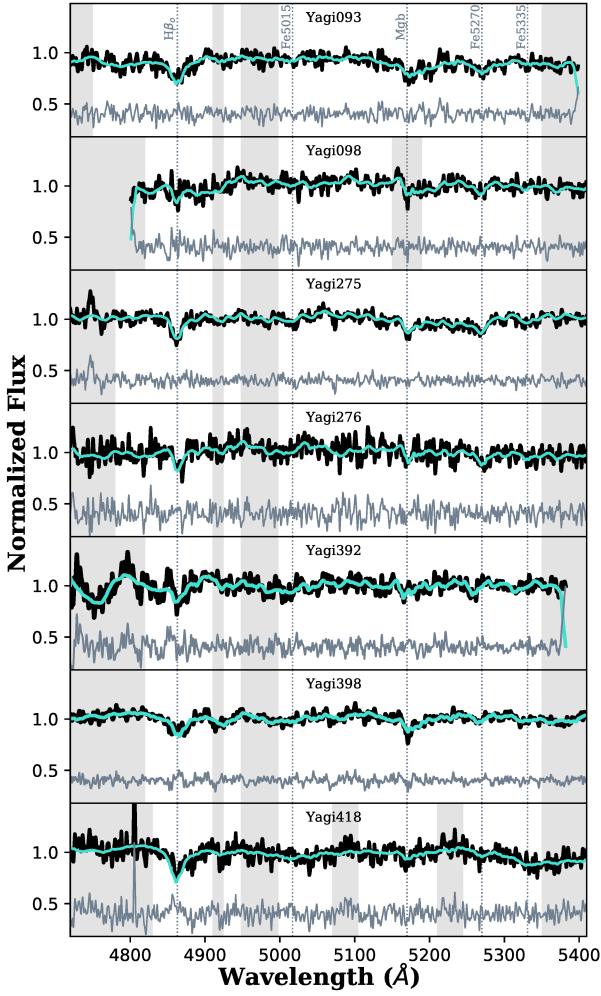


Figure 2. Coma UDG spectra. Reduced spectra for the 7 UDGs presented in this work, highlighting the spectral range used for the stellar population analysis. The spectra and the full spectral fitting result (cyan line) have been normalised for illustration purposes. The grey shaded areas correspond to the masks used in the full spectral-fitting approach and the residuals from the fit are shown at the bottom of each panel in grey. The key line indices used in the index approach have been also labelled and marked by dotted lines.

continuous SFH, as seen in Figure 3. The figure shows the cumulative mass and light derived with STECKMAP and the SFH from STARLIGHT. It is seen that all galaxies show formation histories that extend down to recent times. From the SFHs we can also calculate the timescales for the galaxy to form 50% and 90% of its stellar mass (t_{50} and t_{90} , respectively). Although neither of these values is a direct measurement of the quenching time, a comparison between the timescales to form both can indicate the rate of star formation of the galaxy. From the STECKMAP cumulative mass we can see that our UDGs reached half of their stellar mass on timescales of ~ 2.5 – 5.5 Gyrs. However, the second half of the mass is typically built-up over a rather long timescale of ~ 7 Gyr, reaching their t_{90} about 2–4 Gyrs ago. This implies an extended, steady SFH and late quenching times, with those reaching their half mass mark earlier, ‘quenching’ earlier too (i.e. Yagi 418, Yagi 093 and Yagi 398). If we used the results

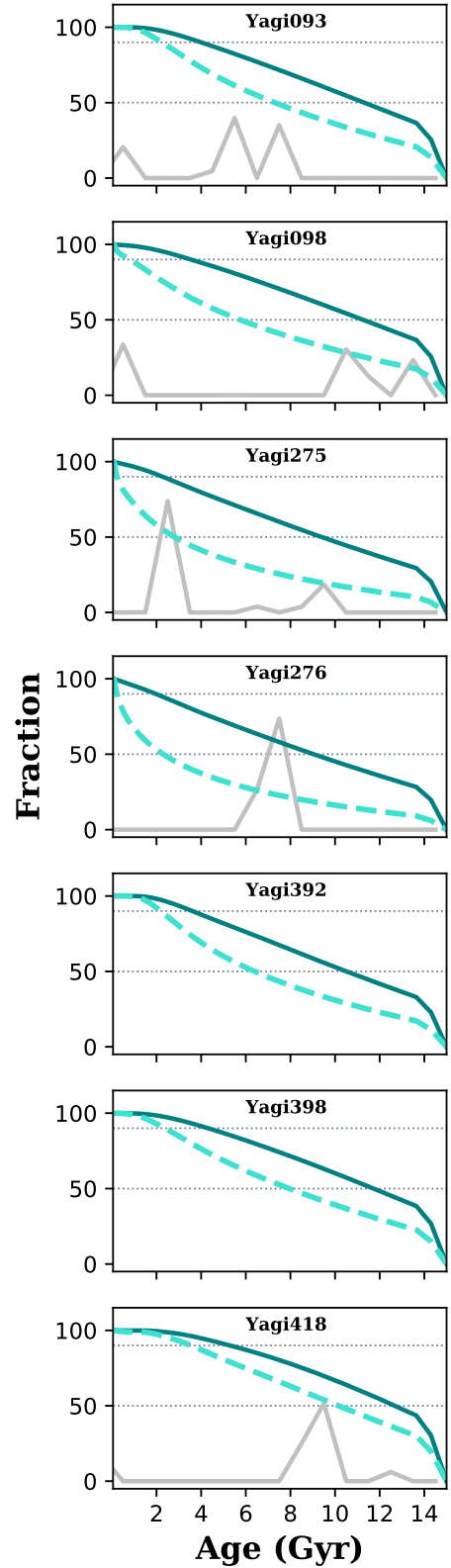


Figure 3. Star formation histories of Coma UDGs. We show the cumulative mass (continuous cyan line) and light (dashed cyan line) from STECKMAP and the derived SFHs from STARLIGHT (grey line) for those UDGs with a good flux-calibration (which is thus lacking for Yagi392 and Yagi398). Each panel shows an individual UDG as labelled, with the created amount of mass/light at a given time. The dashed lines in each panel correspond to 50% and 90% of mass/light created.

from **STARLIGHT**, which give more bursty SFHs (although also extended in time for most of the cases), the average t_{50} and t_{90} are 3.5 and 9 Gyr, respectively, compatible with the **STECKMAP** results. We will further discuss the implications of such quenching timescales later in Section 4.2.

Having a variety of measurements allows for flexibility in the results. This is, depending on the quality of the spectra one can choose which approach is more reliable. For example, if there is a noise spike near an absorption line relevant for the analysis, then the line index approach will not be reliable for that galaxy, while a poor flux calibration will not allow one to trust the derived SFH. A full detailed description of the stellar population analysis and some comparisons within the different methods can be found in the Appendix. After a meticulous inspection of each line-index used and spectral fit quality, we quote in Table 2 the most robust stellar population properties that will be used throughout the following sections. In order to be as consistent as possible, we use the **STECKMAP** values (when possible) for the ages and total metallicities, but the line-index results for the $[\text{Fe}/\text{H}]$ and α -abundances. With these selected stellar populations, we then derive the stellar mass of each UDG using their stellar population mass-to-light (M/L) ratio and the R -band total magnitude.

We find a varied range of stellar population properties from the mean luminosity-weighted values, in particular for the ages and the abundances. The ages of our 7 UDGs cover intermediate to old ages (4–10 Gyr), with a median age of 7.3 ± 2.3 Gyr. All the UDGs in this work have low total metallicities with a median of $[Z/\text{H}] = -0.72 \pm 0.25$ and a median of $[\text{Fe}/\text{H}] = -0.98 \pm 0.84$ dex. The median abundance ratio of $[\text{Mg}/\text{Fe}]$ is 0.16 ± 0.59 , with all of them (except for one) having super-solar values. Unfortunately, both $[\text{Fe}/\text{H}]$ and $[\text{Mg}/\text{Fe}]$ could only be measured for four out of the seven UDGs from the line indices. We additionally examined two other Coma UDGs (Yagi285 (DF25) and Yagi413) in our sample but are not included in the analysis because their S/N was too low for a reliable stellar population analysis. However, to first order they were both consistent with having old ages and low metallicities.

There is, however, a caveat with the use of line indices (and the study of integrated light, in general) to retrieve mean luminosity ages. The existence of old, metal poor ($[Z/\text{H}] \lesssim -1$ dex or $[\text{Fe}/\text{H}] \lesssim -1.5$ dex) bright stars, such as blue horizontal branch (BHB) stars, can mimic the signatures of young stars by boosting the equivalent width of the Balmer lines. In these cases, it is hard to distinguish between a truly young stellar population and an old one that hosts BHB stars. Such an effect has been reported in globular clusters and for some dwarf galaxies in groups (e.g. Monaco et al. 2003; Da Costa et al. 2009; Deason, Belokurov & Weisz 2015) and has been discussed even for more massive galaxies (e.g. Thomas et al. 2005).

Inspecting our spectra we can see that none of the UDGs have a remarkable $\text{H}\beta$ line indicative of young ages, not even for the UDGs that have a mean-luminosity weighted young age. For those UDGs that have metallicities lower than, or similar, to -1 dex and that could potentially be affected by BHB stars, are Yagi398 and Yagi418. They are the oldest UDGs in our sample already, and thus their ages could correspond to lower limits. However, the rest of the UDGs show younger ages but higher metallicities, and thus we assume

that they are not affected by the presence of BHB stars. In fact, if any object could be affected it would be the dwarfs in our sample. With metallicities typically below -1 dex, the majority present intermediate age populations and strong $\text{H}\beta$ features. However, as this is an intrinsic issue in the stellar population models and our dataset lacks the diagnostics necessary to distinguish between the presence of BHB stars and genuinely young ages (i.e. Schiavon et al. 2004), we caution the reader about this caveat but proceed with the measured properties, discussing the implications when necessary.

4 DISCUSSION

We have presented new spectroscopic data for 7 UDGs in Coma, the largest spectroscopic study of the stellar populations of UDGs to date. They are confirmed members of Coma, at a mean $z \sim 0.0223$. They have rather red colours ($B - R \sim 0.94$, an average size of $\langle R_e \rangle \sim 2.3$ kpc and a stellar mass of $\langle M_* \rangle \sim 9.8 \times 10^7 M_\odot$. As given in Table 2, we find a range of stellar population properties for our Coma UDGs, with a median luminosity-weighted age of 7.3 ± 2.3 Gyr, total metallicity of $[Z/\text{H}] = -0.72 \pm 0.25$ and α -abundance ratio of $[\text{Mg}/\text{Fe}] = 0.16 \pm 0.59$. They all present extended SFHs, with a median quenching time (given by the t_{90} formation timescale) of ~ 10 Gyr.

As our aim is to reveal the origin(s) of these galaxies based on their stellar populations we combine our new data with other UDGs from the literature. The latter include spectroscopic data for the three Coma UDGs from G+17 (i.e. DF44, DF17 and DF07), and photometric data for two UDGs from P+17 (i.e. the Virgo member VCC 1287 and the field UDG called DGSATI). We note that all G+17 UDGs are further out from the Coma centre. Both DF07 and DF17 are part of the spectroscopic sample of Kadowaki, Zaritsky & Donnerstein (2017), with four more Coma UDGs located at even larger cluster-centric radii (DF03, DF08, DF30 and DF40). We do not use their results in the following figures because their stellar populations were estimated by visual comparison, but we consider them for the discussion statements. It is worth emphasizing that neither G+17 nor P+17 derived $[\text{Mg}/\text{Fe}]$ ratios but assumed solar values.

Besides including the results from the LLG and HLG galaxies included in our DEIMOS mask, we also use a sample of Coma galaxies from S+09 that inhabit the same area as our UDGs. They were initially selected to represent a red population of dwarf galaxies but they covered a range in luminosities. We therefore apply a similar cut to our LLG and HLG mask galaxies at $R=17$ to separate between dwarf galaxies and more luminous ones. Finally, to extend to more massive objects inhabiting the surrounding areas in the Coma cluster core, we also include a sample of Coma galaxies from Ferré-Mateu et al. (2014) (AFM+14 hereafter). They have been separated morphologically in Sánchez-Blázquez et al. 2006 between early-type galaxies (ETGs) and late-type galaxies (LTGs).

	Method (age/[Z/H])	S/N	Age (Gyr)	[Fe/H] (dex)	[Z/H] (dex)	[Mg/Fe] (dex)	t_{50} (Gyr)	t_{90} (Gyr)	M_* (M_\odot)
Yagi 093	(3)	23	7.88±1.76	-1.48±0.82	-0.72±0.18	0.64±0.25	3.2	10.5	3.05E+08
Yagi 098	(3)	19	6.02±2.56	–	-0.70±0.18	–	3.3	10.6	1.07E+08
Yagi 275	(3)	25	4.63±2.60	-0.06±0.51	-0.37±0.19	-0.42±0.65	4.8	11.6	9.44E+07
Yagi 276	(3)	18	4.24±2.32	–	-0.38±0.71	–	5.3	11.9	1.41E+08
Yagi 392	(3)	15	7.30±2.06	–	-0.39±0.23	–	4.0	10.4	9.08E+07
Yagi 398	(3)	21	8.27±3.14	-0.48±0.87	-0.92±0.38	0.06±0.68	3.0	10.6	3.64E+07
Yagi 418	(3)	18	9.69±2.02	-1.48±0.96	-1.10±0.95	0.27±0.53	2.2	9.4	1.24E+08
Median UDGs			7.32±2.32	-0.98±0.84	-0.72±0.25	0.16±0.59	3.7	10.9	1.1E+08
J125944.10+274607.5	(2)	18	10.12±4.00	-0.90±0.97	-0.80±0.10	-0.06±0.40	2.5	5.5	2.1E+08
J125942.65+274658.8	(1)	15	6.00±2.00	–	-1.68±0.50	–	–	–	1.7E+08
J125948.33+274547.6	(2)	15	7.56±2.00	–	-0.89±0.50	–	3.5	12.5	5.1E+07
J125939.09+274557.5	(2)	18	6.99±1.08	–	-1.67±0.18	–	6.0	6.0	2.4E+08
GMP 2749	(2)	30	6.86±2.65	-0.76±0.49	-1.16±0.09	0.08±0.85	5.5	10.5	2.6E+08
GMP 3519	(2)	25	8.05±1.00	-0.86±0.16	-0.88±0.15	-0.14±0.17	12.5	4.5	6.5E+08
Median LLGs			7.28±2.00	-0.84±0.49	-1.03±0.17	-0.06±0.40	5.5	6.0	2.3E+08
GMP 2800	(2)	40	4.53±0.50	-0.34±0.21	-0.14±0.20	-0.14±0.43	9.5	9.5	1.0E+10
GMP 2923	(1)	38	4.60±0.30	-0.45±0.38	-0.04±0.27	-0.06±0.70	4.0	12.0	9.8E+08
GMP 2945	(2)	40	12.30±4.00	-0.27±0.30	-0.14±0.28	0.08±0.35	1.0	4.5	2.1E+10
GMP 3071	(2)	50	8.65±0.30	-0.63±0.24	-0.19±0.44	0.47±0.43	1.0	11.5	3.7E+09
GMP 3298	(1)	55	3.93±2.40	-0.33±0.12	-0.28±0.11	0.19±0.14	2.5	12.5	5.0E+09
GMP 3493	(2)	53	13.33±2.40	-0.27±0.33	-0.05±0.22	0.27±0.39	0.5	1.0	4.0E+09
Median HLGs			6.63±2.40	-0.34±0.27	-0.15±0.25	0.14±0.41	1.7	10.5	3.9E+09

Table 2. Stellar Population Properties of Coma Galaxies. The table presents the most robust results for the stellar population properties, as discussed in the Appendix. First column specifies the method used to derive the luminosity-weighted ages and total metallicities (1=line-indices; 2=STARLIGHT; 3=STECKMAP), whereas [Fe/H] and [Mg/Fe] values are always derived from the line indices. The derived S/N within the spectral coverage used for the full-spectral-fitting and the derived quenching times (represented by t_{50} and t_{90} , this is the time it takes since the Big Bang for the galaxy to build up 50 and 90 % of its mass) are also quoted, together with the stellar mass calculated with the stellar population M/L ratios.

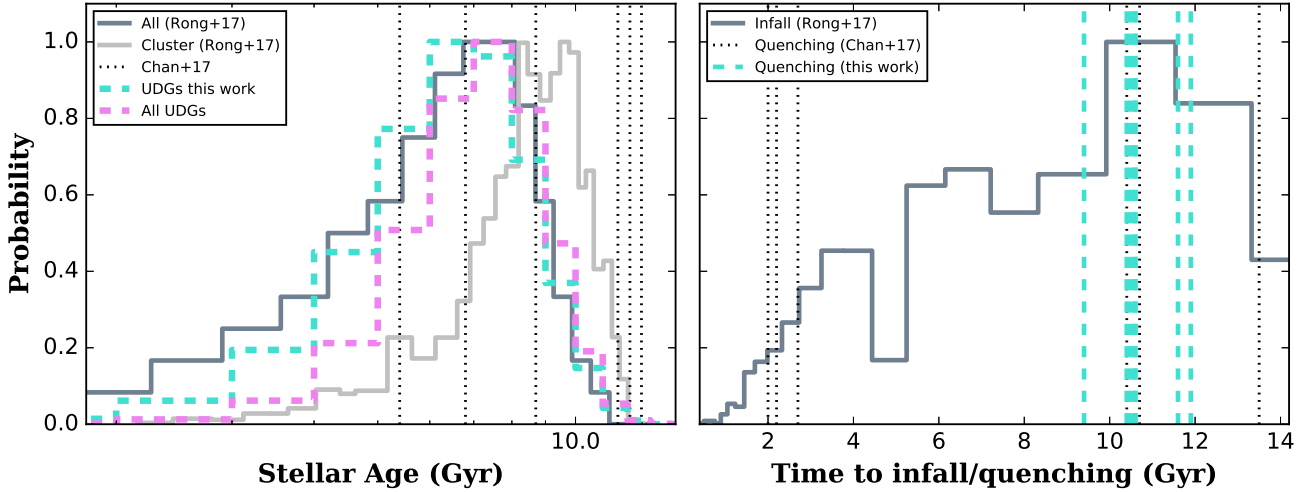


Figure 4. Theoretical predictions for UDGs. *Left panel:* The theoretical age distribution for UDGs from the simulations of Rong et al. (2017), as expected if UDGs are dwarf-like galaxies. The dark grey histogram represents the distribution for all the simulated UDGs (cluster+field) whereas the light grey one corresponds to only cluster UDGs. The dotted black lines show the ages of the simulated UDGs in Chan et al. (2017). Super-imposed we show the observed distribution of ages for our 7 Coma UDGs (dashed cyan histogram) and the distribution if we include other literature UDGs from G+17 and P+17 (dashed purple histogram). *Right panel:* Predictions for the infall time of the Rong et al. 2017 UDGs (grey histogram), showing that their simulated UDGs tend to have late infalling times. Overlaid are the quenching times for UDGs from the Chan et al. 2017 simulations and the t_{90} for our UDGs. Even if there is a ~ 1.5 –2 Gyr delay between the time of infall and the galaxy quenching (e.g. Muzzin et al. 2008; Haines et al. 2015), all our UDGs are compatible with a late infall into the cluster environment.

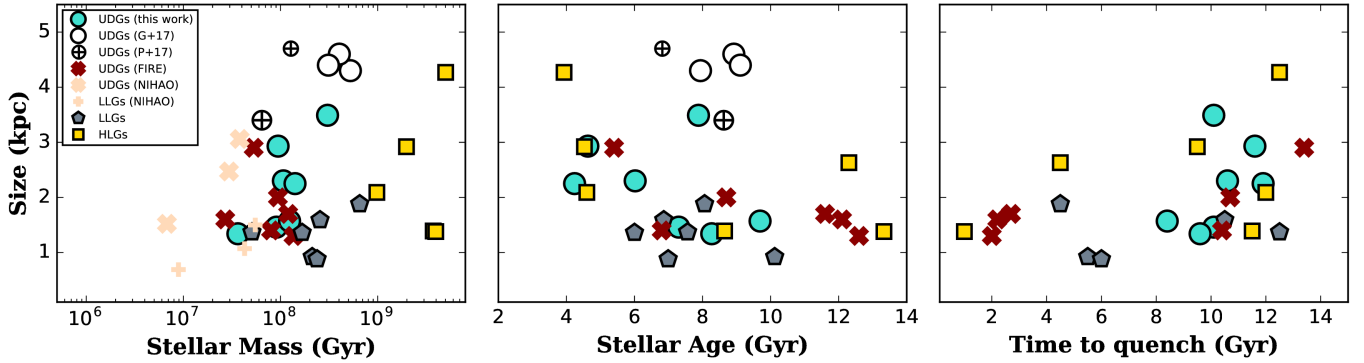


Figure 5. Sizes of simulated and observed UDGs. *Left panel* shows the mass–size relation for the simulated UDGs in both FIRE (red crosses; Chan et al. 2017) and NIHAO (pink crosses; Di Cintio et al. 2017) simulations. We compare them to the galaxies in Coma from our mask: UDGs (cyan circles), dwarf galaxies (grey pentagons) and HLG galaxies (yellow squares). We also include other literature UDGs (open circles for G+17; crossed open circles for P+17, with DGSAT I as a smaller symbol to show it is a field UDG rather than a cluster one). *The middle panel* shows the age–size relation presenting a trend where younger UDGs have more extended sizes due to their later infall. *The right panel* emphasises the age trend by showing that galaxies with longer quenching timescales are larger. Interestingly, neither Yagi 093 nor any of the other literature UDGs are reproduced by the simulations, pointing to a different formations scenario for these UDGs.

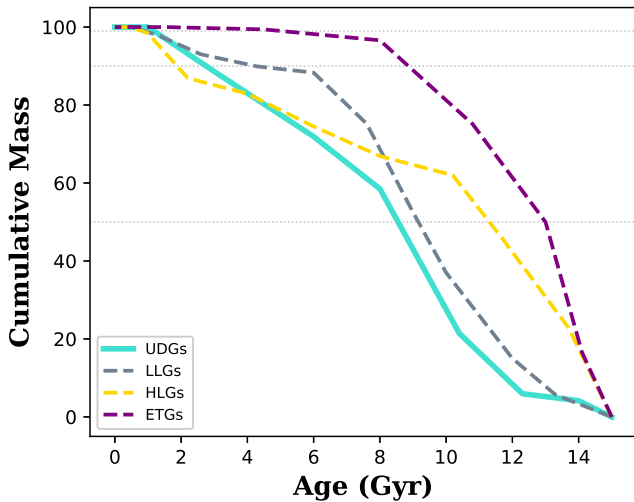


Figure 6. Mass assembly of Coma galaxies. The averaged SFHs for the different galaxy classes in Coma are translated into the cumulative stellar mass, to show the different formation timescales the galaxies undergo. Therefore the three horizontal dotted lines mark the creation of 50%, 90% and 99% of stellar mass. Our UDGs (cyan continuous line) present steady and extended SFHs, with late formation epochs and not quenching until ~ 3 Gyr ago. The LLGs in the mask (grey dashed line) seem to follow the UDGs timescales closely, albeit they quench ~ 2 Gyr earlier, compatible with the theoretical model of Rong et al. (2017). In contrast, both massive ETGs and normal HLG galaxies show early formation epochs.

4.1 Comparison with other literature

Our results are consistent with the results from G+17 for three UDGs in the outer regions of the Coma cluster: DF7 (with $7.9^{+3.6}_{-2.5}$ Gyr and $[\text{Fe}/\text{H}] = -1.0^{+0.3}_{-0.4}$); DF44 (with $8.9^{+4.3}_{-3.3}$ Gyr and $[\text{Fe}/\text{H}] = -1.3^{+0.4}_{-0.4}$); and DF17 (with $9.1^{+3.9}_{-5.5}$ Gyr and $[\text{Fe}/\text{H}] = -0.8^{+0.5}_{-0.5}$). Similar ages but somewhat lower metallicities have been also reported for a Virgo

UDG, VCC 1287 (with a lower limit age of 8.6 Gyr and lower limit $[\text{Z}/\text{H}] = -1.55$; P+17). Similarly low metallicities have also been found to be the best match for the 4 UDGs from Kadowaki, Zaritsky & Donnerstein (2017), although they only report their stacked spectra to be mostly compatible with a very old SSP. On the contrary, a higher metallicity of $[\text{Z}/\text{H}] = -0.63^{+0.35}_{-0.62}$ has been reported for a field UDG, DGSAT I (P+17), with a younger age of $6.81^{+4.08}_{-3.02}$ Gyr that indicates a somewhat extended SFH, which is very similar to our UDG results.

4.2 Comparison with theoretical predictions

We find that UDGs (including literature ones) show a range of stellar ages regardless of the methodology used, from ~ 4 – 10 Gyr. We now look at how this age distribution compares with the theoretical predictions. Figure 4 shows the observed age distribution for our sample of UDGs alone (cyan dashed histogram) and including the literature ones (purple dashed histogram). The simulated FIRE UDGs of Chan et al. (2017) have their ages marked as vertical dotted lines. The continuous histograms correspond to the theoretical prediction models from Rong et al. (2017), both for the entire UDG population (dark grey, skewed towards low density environments) and only for the cluster environment (light grey). The figure shows an age distribution for our UDGs peaking at ~ 7 –8 Gyr (which corresponds to a redshift of formation of $z \sim 1$) that is strikingly similar to the simulated UDGs of all environments. However, the distribution of cluster UDGs in the simulations are slightly older with a mean age of ~ 9 Gyr. As mentioned above, there is the possibility that some of the measured ages might be a lower limit due to the BHB star presence. This could shift the observed UDGs towards slightly older ages, better matching the simulated cluster distribution. We thus conclude that our UDGs reveal a range of ages that correspond to a redshift of formation of $z \lesssim 1$. This would, therefore, exclude any of the scenarios that expect very old ages (i.e. the ‘failed’ galax-

ies scenario), where formation redshifts of at least $\gtrsim 2$ are expected.

As the mean luminosity-weighted ages can be biased towards younger bursts of star formation, we also look at the predictions from the quenching times due to the infall into the cluster environment. The right panel of Figure 4 shows the predicted distribution of infall time into the cluster from Rong et al. (2017), showing typically very late timescales for their simulated UDGs (~ 10 Gyr). We also overlay the quenching times used in the simulated FIRE UDGs. This quenched time does not represent directly the infall time, as quenching may take ~ 1.5 –2 Gyr after infall (e.g. Haines et al. 2015; Muzzin et al. 2008). In fact, such a quench can occur by internal processes before infall (e.g. as described by Di Cintio et al. 2017 to explain field UDGs) or be caused by external processes during the infall. In the FIRE simulations the gas removal mechanism is not specified but they assume that the hot gas reservoir in the feedback-expanded dwarfs will be removed by ram pressure stripping, while suffering strangulation or a feedback episode as they fall into the clusters. This will quench star formation and turn the UDG into a redder galaxy. In order to test both scenarios (dwarf-like *vs* ‘failed’ galaxy) they allowed for a wide range of quenching times (and thus ages), with some galaxies quenching very early (~ 2 Gyr) and some late ones (~ 11 Gyr). We also overlay our UDGs with cyan vertical lines. What we have considered the quenching time for them is their t_{90} . This is because in Section 3 we proved that the SFHs of our UDGs are sustained over time, forming the second part of their mass in timescales even longer than the first half. Should they have fallen into the cluster earlier, that would have quenched and stopped such a star forming rate earlier. The figure shows that all our UDGs are compatible with the distribution of Rong et al. (2017) with late infalls, even if we correct for the delay between infall and quenching (i.e. 1.5–2 Gyr). These results are also in agreement with the infall times reported in Paper I from a velocity phase-space analysis.

Figure 5 shows a comparison with both simulated UDGs from FIRE (Chan et al. 2017) and NIHAO (Di Cintio et al. 2017) in terms of the size of UDGs. Note that while we can directly compare to the FIRE simulations as they allow their galaxies to quench at different times due to cluster infall, those in NIHAO are purely for field galaxies and therefore not quenched by infall. However, if our findings of late infall into Coma are correct, where UDGs were mostly developed outside and only quenched recently, the results should not depart extremely. The left panel shows the stellar-mass relation, which shows the well established trend of more massive galaxies being larger. Our UDGs (and the Virgo one) are compatible with the FIRE simulations although they are, on average, larger than the NIHAO ones. The other literature UDGs from G+17 and DGSATI show instead larger sizes and are more massive, indicating that a different path of formation for them might be necessary. The middle and right panels of Figure 5 emphasise the two types of simulated UDGs reproduced by the FIRE simulations: one that quenches at earlier epochs and thus has old ages, another that is free to evolve and quenches at later times, therefore with younger ages. The trend is that older galaxies are smaller: they had less time in the ‘dwarf’-regime before they are quenched, whereas as the quenching time becomes longer, galaxies become more extended. Our UDGs seem

to follow such trends, matching the areas populated by the late-quenched galaxies from FIRE. However, Yagi 093 and the other literature UDGs do not follow the expected trend, with sizes larger than what expected by their stellar age, further suggesting a different pathway of formation.

We remind the reader that this is only a qualitative assessment of the formation timescales of our UDGs and that the message that is obtained is that our Coma UDGs have star formation histories compatible with being late infalls in the Coma cluster, as they present sustained rates of star formation until to very recently. This is clear from Figure 6, which shows the averaged SFH for our UDGs, compared to the averaged SFHs of the other masks galaxies (LLGs and HLGs) and the massive ETGs in AFM+14. Their different formation histories are clear in this figure. Both massive ETGs and HLGs start building up their masses at the earliest epochs with high star formation rates and reach their t_{50} in less than ~ 1 and 3 Gyr, respectively. In stark contrast, both our control dwarf galaxies and UDGs start building up their mass very slowly initially, only starting to have significant star formation rates after 1–2 Gyr. Neither UDGs nor dwarf galaxies reach their t_{50} until past ~ 6 and 5 Gyr, respectively. Dwarf galaxies seem reach their t_{90} 5 Gyr ago whereas our UDGs do not reach such mass until ~ 3 Gyr ago. This difference in ~ 2 Gyr between the ‘quenching times’ is the same as the difference in the infall time between UDGs and the dwarf galaxies of Rong et al. (2017) further reinforcing the late infall scenario. The question that arises now is if the location within the cluster is compatible with such recent infall times.

4.3 Stellar populations dependence on cluster-centric radius

We next study if there is any dependence of the properties with cluster-centric radius that could provide a hint about the infalling/quenching times. Figure 7 shows the mean luminosity-weighted age and total metallicity with projected distance for our sample of DEIMOS Coma UDGs, the G+17 UDGs, the rest of the DEIMOS mask control galaxies and the S+09 and AFM+14 samples. The [Fe/H] values from G+17 have been transformed into total metallicities in order to be included in this figure, assuming a [Mg/Fe] ~ 0.1 (the expected abundance following Thomas et al. 2005 and similar to our median value, see below). Similarly, the [Fe/H] of S+09 have also been converted to total metallicities, in this case using their published [Mg/Fe] values. Our UDGs are all located at 300 pc, compatible with the radius of innermost survivability for UDGs (e.g. van Dokkum et al. 2015a; van der Burg, Muzzin & Hoekstra 2016).

The top panel shows that galaxies further from the cluster centre tend to be younger, emphasised by the LLGs of S+09. The latter reported a spread in ages of 2–10 Gyr, with the oldest galaxies populating the central regions of the cluster. Our Coma UDGs also mildly reproduce such a trend, despite not having a wide radial range coverage and not reaching the innermost regions. In fact, this effect could be even more drastic if we consider that the oldest of our UDGs are a lower limit due to the BHB issue. Interestingly, the G+17 Coma UDGs, located at further distances, behave the opposite way than the outer dwarfs, remaining basically old.

The lower panel shows no trend in metallicity with projected distance, only a mild trend with galaxy type, with UDGs having slight lower metallicities but similar stellar ages to their co-spatial S+09 LLGs and our mask HLGs. These difference in metallicities can be interpreted as the result of the harsh cluster environment being more effective at stripping the UDGs as opposed to dwarfs and more massive systems, having less time for self-enrichment that leaves them with low metallicities (see discussion below). We find again a different behaviour for the UDGs from G+17, showing a trend with lower metallicities as they are further from the cluster centre as opposed to the co-spatial LLGs. This result is also reinforced by the low metallicities of Kadowaki, Zaritsky & Donnerstein (2017) UDGs at even further radii.

The initial question in the section was if the recent infall times were compatible with the location of the UDGs within the cluster. Compared to other co-spatial galaxies, we have found them to be less metallic and in some cases with young ages that could, in principle not reconcile with being a recent infall and being located near the centre at the same time. However this can be explained if the position of our UDGs in 3D is not the same to the other galaxies, particularly in the core where the number of UDGs is known to decrease significantly (e.g. van der Burg, Muzzin & Hoekstra 2016; Lee et al. 2017). Our central UDGs could be at larger 3D distances than the other central galaxies at a similar projected 2D radius (and therefore should not be considered co-spatial in 3D), having therefore fallen into the cluster at later times than the LLGs and more massive systems, which is compatible with the SFHs in Figure 6.

4.4 Scaling relations: clues to the origin of UDGs in Coma

Figure 8 shows the relation between the derived stellar population properties presented in the previous sections for our UDGs and the control galaxies. We remind the reader that in general, LLGs are more representative of dwarf galaxies (only one of them is spiral), whereas HLGs are mostly spiral-like galaxies. The top panel shows the age–metallicity plane, with a trend of older UDGs having lower metallicities, which is further emphasised if we consider the effect of BHB stars for the lowest metallicity galaxies (some of our dwarf galaxies and two of the UDGs). The S+09 dwarf galaxies also show a similar decreasing trend of metallicity with age, which is not seen neither for the HLGs nor the ETGs.

Typically, α -abundances have been interpreted on the basis of how fast the galaxy forms half of its stellar mass (e.g. Thomas et al. 2005; de La Rosa et al. 2011; McDermid et al. 2015), what we have measured as t_{50} . We have seen that our UDGs are mostly compatible with accomplishing this 50% of the stellar mass in relatively fast timescales (3–4 Gyr), which could explain them having enhanced abundance patterns. Although we were not able to obtain the abundances for all the UDGs, we can see that the only UDG with an α -abundance lower than the rest (Yagi275) is the one with younger ages, showing an extended SFH with a large contribution of recent star formation. In contrast, Yagi093 and Yagi418 both show an enhanced pattern that would indicate early formation. As $[\text{Mg}/\text{Fe}]$ – $[\text{Fe}/\text{H}]$ is understood as a proxy for the self-enrichment of the galax-

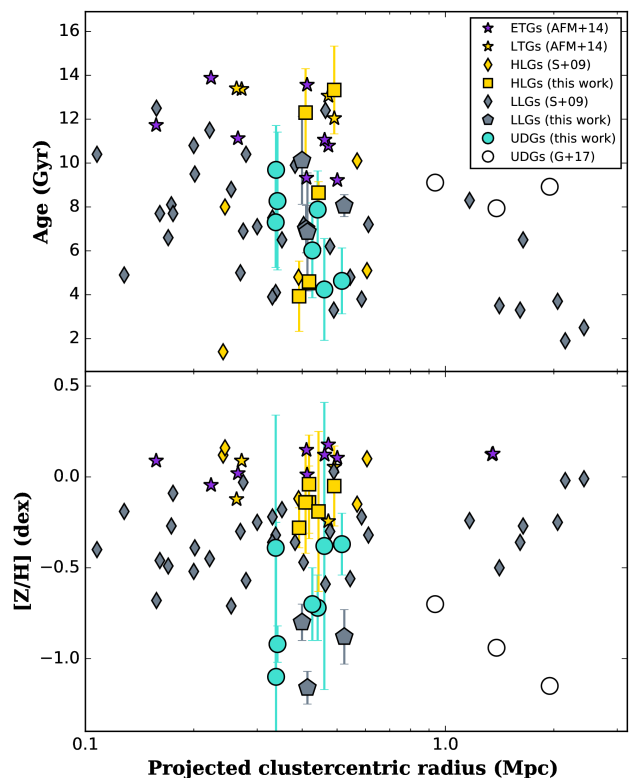


Figure 7. Stellar population properties of UDGs with projected cluster–centric radius. *Top:* The mean luminosity-weighted ages of our Coma UDGs are plotted as cyan circles, while the G+17 Coma UDGs are shown as open circles. Our Coma mask LLG and HLG galaxies are shown as grey pentagons and yellow squares, respectively. We have separated the AFM+14 sample into ETGs (purple stars) and LTGs (yellow stars). The sample of red Coma dwarf galaxies from S+09 has also been separated according to a luminosity cut of R -band magnitude $R=17$, with LLGs as grey diamonds and HLGs as yellow diamonds. The objects in the outskirts tend to show younger mean-luminosity-weighted ages, with a strong variation for the S+09 dwarfs. Our Coma UDGs also seem to follow this trend, with the two youngest ones being further from the centre, but such trend is not followed by the outermost UDGs of G+17. *Lower panel:* Following the same colour and symbol scheme as above, this panel shows no trend of the total metallicity with cluster–centric radius. However, if we consider inner and outer UDGs, there is a trend of UDGs being more metal poor at larger projected distances.

ies, reflecting the different timescales of nucleosynthesis from different type of supernovae, the lower panel of Figure 8 explores such correlation. It is seen that those having higher $[\text{Mg}/\text{Fe}]$ ratios are those exhibiting the lowest $[\text{Fe}/\text{H}]$, compatible with not having had time to be as much enriched in subsequent star formation episodes from more metal-rich gas. This is what is seen for ultra-faint dwarfs (e.g. Frebel, Simon & Kirby 2014) and Local Group dwarf and dwarf spheroidal galaxies (e.g. Venn et al. 2004; Kirby et al. 2011; Revaz & Jablonka 2018), with $[\text{Fe}/\text{H}]$ – α ratios similar to Milky–Way field stars, whereas some of our UDGs (the most enhanced ones) have similar abundances to Milky–Way halo stars (e.g. Venn et al. 2004).

The final step in the analysis is to see how the stellar populations of our UDGs correlate with their stellar mass

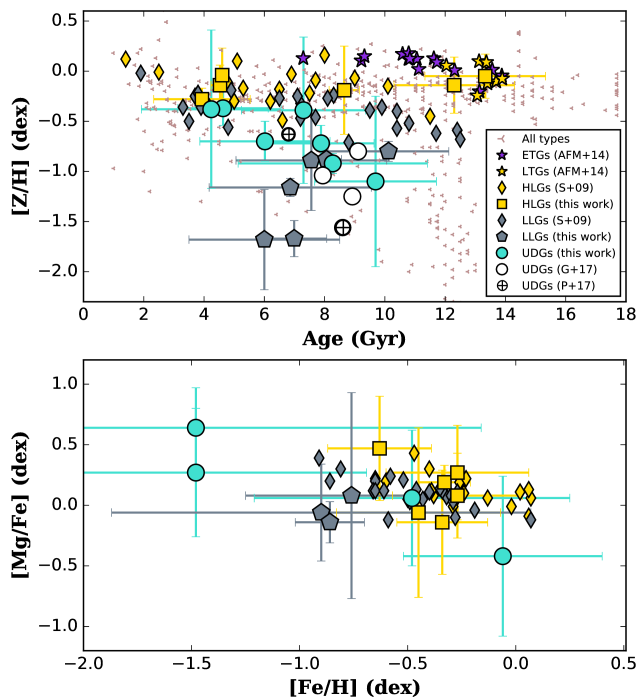


Figure 8. Stellar populations of UDGs. *Top panel* shows the age–metallicity distribution of our Coma UDGs, literature ones and the control galaxies from both the observed mask and literature. Colour and symbols scheme is as in Figure 7 but now we also include the Virgo and field UDGs of P+17 (crossed open circles, where the smaller one corresponds to the field UDG to emphasise its different environment). Both the red dwarf galaxies of S+09 and our UDGs show a trend where older galaxies have lower total metallicities. *Lower panel:* [Mg/Fe]–[Fe/H] relation, a proxy for the self-enrichment of a galaxy. Our UDGs with the lowest [Fe/H] values are those with the higher α -element abundances, which can be indicative of a faster star formation.

and to find out if their location in such relations can shed any further light into the origin(s) of UDGs. In Figure 9 we show the age, metallicity and α -element abundance ratio against stellar mass for both Coma and other literature UDGs, the DEIMOS mask control sample and both the S+09 dwarf and AFM+14 massive galaxies samples. The stellar masses for the S+09 sample have been converted from the luminosity, r -band magnitude and the M/L ratio corresponding to their SSP age and metallicity, consistently as we measured the stellar masses in Section 3 for our DEIMOS objects, using the MILES SSP models. Before proceeding we remind the reader the caveat that all galaxies are not from the same environment/location within the cluster. However, only a few of the S+09 LLGs are located at further radii similar to the UDGs from G+17, and we note that both UDGs from P+17 belong to either another cluster or the field.

The top panel includes the mass–age relation for massive systems from Thomas et al. (2005). The stellar ages of UDGs are slightly lower than the outermost UDGs of G+17, except for Yagi 093, as mentioned above. However, they are similar to the UDGs in P+17 (both cluster and field UDGs) and to LLGs in our DEIMOS mask. The HLGs in the mask show a wider spread in ages, similar to the one seen for the S+09 sample. This panel shows that the ages of the UDGs

are consistent with the mass–age relation of massive systems if such a relation was extrapolated to lower masses.

The middle panel of Fig. 9 shows the well-known mass–metallicity relation, represented by Gallazzi et al. (2005) for high mass galaxies and by Kirby et al. (2013) for low-mass ones. Typically, our UDGs lie above the mass–metallicity relation expected for low-mass systems of Kirby et al. (2013). In fact, our UDGs seem to rather follow the low-mass end of the Gallazzi et al. (2005) relation, following the tail described by the Coma LLGs from S+09, presenting slightly lower metallicities than the latter. S+09 already reported that such galaxies seemed to follow the mass–metallicity relation of more massive galaxies rather than the lower mass systems of Kirby et al. 2013, in agreement with our findings for the UDGs and some LLGs in our mask. The UDG that strongly departs from the rest is the Virgo UDG VCC 1287, which has similar old ages but lower metallicity (P+17).

The lower panel of Fig. 9 shows the relation of the stellar mass with [Mg/Fe]. Our UDGs have a median value of [Mg/Fe] ~ 0.16 dex, although the scatter in this relation is quite large and also the errors in the measurement. However, this median value is compatible with the relation for normal galaxies from Thomas et al. (2005) extrapolated to lower stellar masses. Such abundances are similar to those found for other low-mass galaxies and compact stellar systems such as ultra compact dwarfs and compact ellipticals (e.g. Janz et al. 2016; Ferré-Mateu et al. 2018). This would support the claim that some compact stellar systems could be the remnant nuclei of clumpy UDGs that have the bulk of their stellar content stripped during their journey across the cluster environments (Janssens et al. 2017). As already pointed out above, both UDGs with super-solar abundances are those with the lowest values of [Fe/H], which can be understood in terms of a strong suppression of the Fe rather than an over-abundance of Mg as typically seen in more massive, enhanced galaxies. It would be very interesting to see what are the [Mg/Fe] ratios (and quenching timescales) of the other literature UDGs that seem to be similar to Yagi 093 in other properties and include them in this figure. This topic will be further discussed in Martín-Navarro et al. (in prep) and therefore we do not speculate any further here, as we lack the data quality to address this issue.

We have thus seen that all the properties of our UDGs are most compatible with our observed LLGs (which are typically dwarf galaxies) and in general with the LLGs from S+09 (which are also, typically red dwarfs). This supports the idea that the UDGs studied in this work share a common origin, where they were created outside the cluster environment as dwarf galaxies. Our results also reinforce such a dwarf-like nature for the Virgo UDG VCC 1278 (Beasley et al. 2016) and DF17 (e.g. Peng & Lim 2016; Beasley & Trujillo 2016). However, our data can not discriminate whether these UDGs have extended sizes due to internally driven-processes (i.e. outflow-driven gas feedback Di Cintio et al. 2017) or simply because they lived in high-spin haloes that prevented them from condensing (e.g. Amorisco & Loeb 2016; Rong et al. 2017).

Such dwarf-like origin is consistent for all of our UDGs that populate the central region of Coma, except for Yagi 093. This UDG shows some signs of tidal in-

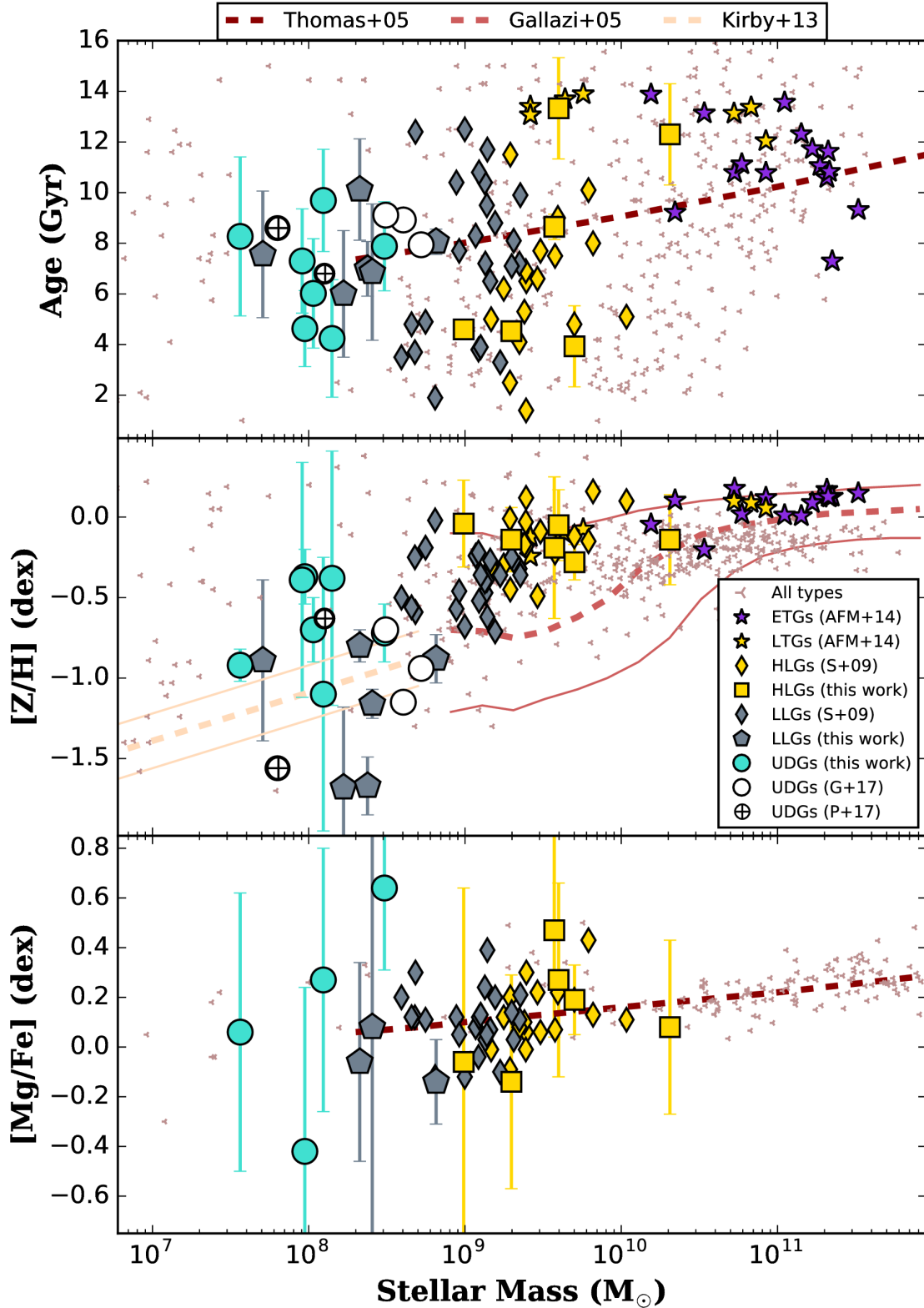


Figure 9. Stellar population properties vs stellar mass. *Top* panel presents the mass–age relation from [Thomas et al. \(2005\)](#), which is known to have a high spread as visible by the background red points (all types of literature galaxies from [Janz et al. 2016](#)). Colours and symbols are as in [Figure 5](#). *Middle* panel shows the mass–metallicity relation for both high mass ([Gallazzi et al. 2005](#)) and low mass galaxies ([Kirby et al. 2013](#)). *Lower* panel shows the [Mg/Fe] overabundance ratio with stellar mass relation from [Thomas et al. \(2005\)](#). In each panel, the UDGs have stellar population properties that are, to first order, consistent with the scaling relations of normal galaxies if they were extrapolated to lower masses, mostly sharing the same properties as the dwarfs in Coma.

interactions and seems to have followed a different formation channel that could be similar to the one necessary to explain the properties of other Coma UDGs at larger cluster-centric radii (e.g. DF44, DF07 and the Kadowaki, Zaritsky & Donnerstein 2017 UDGs). This is compatible with the results in Paper I, where a few UDGs (Yagi 093 included) were shown to be compatible with being primordial galaxies. Therefore, we hypothesize that Yagi 093 would be more similar to DF44, which so far seems to be the best example for a ‘failed’ galaxy. DF44 has been reported to have a large over-abundance of globular clusters and a high velocity dispersion (van Dokkum et al. 2016; van Dokkum et al. 2017), supporting the idea that this UDG must live in a high dark matter halo.

Not having yet solved the relative proportions of dwarf-like and primordial-like UDGs in Coma, this leaves the enigma of the nature of UDGs still open to debate. Future work should be able to tackle this issue by compiling a large, statistical sample of UDGs at different cluster-centric radius with high enough S/N to alleviate the several caveats we encountered during the analysis. This will help put further constraints on the (diverse) origin(s) of UDGs and their relative importance in the cosmological models.

5 CONCLUSIONS

We have presented a new spectroscopic study of the stellar content of 7 UDGs nearby the core of the Coma cluster, the largest to date, in order to further investigate the possible origin(s) of UDGs. The analysis of their stellar ages, metallicities, [Mg/Fe] abundances and SFHs, combined with similar data in the literature, indicates that the UDGs in our sample were accreted into the Coma cluster later than other luminous galaxies and normal dwarfs, being compatible with a rather recent infall. Our UDGs have intermediate ages (~ 7 Gyr), low metallicities ($[Z/H] \sim -0.7$) and slightly super-solar α -abundances ($[Mg/Fe] \sim +0.16$). We find that in general, all their stellar population properties are consistent with the low-luminosity galaxies in our sample, which are mostly dwarfs, and other co-spatial dwarfs from S+09. In fact, UDGs seem to follow most of the higher-mass galaxies scaling relations (i.e. a continuation of mass-age, mass-metallicity and mass- α elements), further supporting their dwarf-like origin.

The mean (luminosity) ages obtained from the different approaches used in this work are also consistent with the predicted age distributions of UDGs from the cosmological simulations of Chan et al. (2017) and Rong et al. (2017), with formation redshifts of $z < 1$. Their sustained star formation rates down to recent times further support the assumption of a late infall into the cluster core, with ‘quenching’ timescales of $t_{90} \sim 10$ Gyr. These results from the stellar populations are further reinforced by the results in Paper I of the series, where recent infall into the cluster has also been found for most of our Coma UDGs. This therefore disfavours the scenarios whereby early-forming primordial galaxies failed to evolve and rather supports the dwarf-like origin for this sample of Coma UDGs. The only exception is Yagi 093, a UDG with some signs of interaction that seemingly followed a different formation pathway more similar to that invoked for larger and more massive UDGs such as DF44.

To summarise, our stellar population results for 7 UDGs in the Coma cluster contribute to the growing evidence towards a dwarf-like origin for most UDGs in the literature. However, the properties of other studied UDGs invoke the need for other formation pathways, leaving the enigma of the nature of UDGs as an open question.

ACKNOWLEDGEMENTS

The authors would like to thank P. van Dokkum and C. Conroy for insightful discussions. AFM and DAF acknowledge the ARC for financial support via DP160101608. AJR was supported by NSF grant AST-1616710 and as a Research Corporation for Science Advancement Cottrell Scholar. JB, BA and IMN were supported by NSF grant AST-1616598. SB was supported by the AAO PhD top-up Scholarship. The data presented herein were obtained at the W. M. Keck Observatory, which is operated as a scientific partnership among the California Institute of Technology, the University of California and the National Aeronautics and Space Administration. The Observatory was made possible by the generous financial support of the W. M. Keck Foundation. The authors wish to recognise and acknowledge the very significant cultural role and reverence that the summit of Maunakea has always had within the indigenous Hawaiian community. We are most fortunate to have the opportunity to conduct observations from this mountain.

REFERENCES

- Amorisco N. C., Loeb A., 2016, *MNRAS*, 459, L51
- Beasley M. A., Romanowsky A. J., Pota V., Navarro I. M., Martinez Delgado D., Neyer F., Deich A. L., 2016, *ApJ*, 819, L20
- Beasley M. A., Trujillo I., 2016, *ApJ*, 830, 23
- Bellazzini M., Belokurov V., Magrini L., Fraternali F., Testa V., Beccari G., Marchetti A., Carini R., 2017, *MNRAS*, 467, 3751
- Burkert A., 2017, *ApJ*, 838, 93
- Cervantes J. L., Vazdekis A., 2009, *MNRAS*, 392, 691
- Chan T. K., Kereš D., Wetzel A., Hopkins P. F., Faucher-Giguère C.-A., El-Badry K., Garrison-Kimmel S., Boylan-Kolchin M., 2017, *ArXiv e-prints*: 1711.04788
- Cid Fernandes R. et al., 2014, *A&A*, 561, A130
- Cid Fernandes R., Mateus A., Sodré L., Stasińska G., Gomes J. M., 2005, *MNRAS*, 358, 363
- Cooper M. C., Newman J. A., Davis M., Finkbeiner D. P., Gerke B. F., 2012, *spec2d: DEEP2 DEIMOS Spectral Pipeline*. Astrophysics Source Code Library
- Da Costa G. S., Grebel E. K., Jerjen H., Rejkuba M., Sharina M. E., 2009, *AJ*, 137, 4361
- Dalcanton J. J., Spergel D. N., Gunn J. E., Schmidt M., Schneider D. P., 1997, *AJ*, 114, 635
- de La Rosa I. G., La Barbera F., Ferreras I., de Carvalho R. R., 2011, *MNRAS*, 418, L74
- Deason A. J., Belokurov V., Weisz D. R., 2015, *MNRAS*, 448, L77
- Di Cintio A., Brook C. B., Dutton A. A., Macciò A. V., Obreja A., Dekel A., 2017, *MNRAS*, 466, L1
- Ferré-Mateu A., Forbes D. A., Romanowsky A. J., Janz J., Dixon C., 2018, *MNRAS*, 473, 1819
- Ferré-Mateu A., Sánchez-Blázquez P., Vazdekis A., de la Rosa I. G., 2014, *ApJ*, 797, 136
- Ferré-Mateu A., Vazdekis A., de la Rosa I. G., 2013, *MNRAS*, 431, 440

Frebel A., Simon J. D., Kirby E. N., 2014, *ApJ*, 786, 74
 Gallazzi A., Charlot S., Brinchmann J., White S. D. M., Tremonti C. A., 2005, *MNRAS*, 362, 41
 Gu M. et al., 2017, *ArXiv e-prints*: 1709.07003
 Haines C. P. et al., 2015, *ApJ*, 806, 101
 Impey C., Bothun G., Malin D., 1988, *ApJ*, 330, 634
 Janssens S., Abraham R., Brodie J., Forbes D., Romanowsky A. J., van Dokkum P., 2017, *ApJ*, 839, L17
 Janz J. et al., 2016, *MNRAS*, 456, 617
 Jones M. G., Papastergis E., Pandya V., Leisman L., Romanowsky A. J., Yung L. Y. A., Somerville R. S., Adams E. A. K., 2017, *ArXiv e-prints*: 1712.01855
 Kadowaki J., Zaritsky D., Donnerstein R. L., 2017, *ApJ*, 838, L21
 Kirby E. N., Cohen J. G., Guhathakurta P., Cheng L., Bullock J. S., Gallazzi A., 2013, *ApJ*, 779, 102
 Kirby E. N., Cohen J. G., Smith G. H., Majewski S. R., Sohn S. T., Guhathakurta P., 2011, *ApJ*, 727, 79
 Koda J., Yagi M., Yamanoi H., Komiyama Y., 2015, *ApJ*, 807, L2
 Kuntschner H. et al., 2010, *MNRAS*, 408, 97
 Lee M. G., Kang J., Lee J. H., Jang I. S., 2017, *ApJ*, 844, 157
 Leisman L. et al., 2017, *ApJ*, 842, 133
 Makarov D. I., Sharina M. E., Karachentseva V. E., Karachentsev I. D., 2015, *A&A*, 581, A82
 Martínez-Delgado D. et al., 2016, *AJ*, 151, 96
 McDermid R. M. et al., 2015, *MNRAS*, 448, 3484
 Merritt A., van Dokkum P., Danieli S., Abraham R., Zhang J., Karachentsev I. D., Makarova L. N., 2016, *ApJ*, 833, 168
 Mihos J. C. et al., 2015, *ApJ*, 809, L21
 Monaco L., Bellazzini M., Ferraro F. R., Pancino E., 2003, *ApJ*, 597, L25
 Mowla L., van Dokkum P., Merritt A., Abraham R., Yagi M., Koda J., 2017, *ApJ*, 851, 27
 Muñoz R. P. et al., 2015, *ApJ*, 813, L15
 Muzzin A., Wilson G., Lacy M., Yee H. K. C., Stanford S. A., 2008, *ApJ*, 686, 966
 Ocvirk P., Pichon C., Lançon A., Thiébaud E., 2006, *MNRAS*, 365, 74
 Okabe N., Futamase T., Kajisawa M., Kuroshima R., 2014, *ApJ*, 784, 90
 Pandya V. et al., 2017, *ArXiv e-prints*: 1711.05272
 Papastergis E., Adams E. A. K., Romanowsky A. J., 2017, *A&A*, 601, L10
 Peng E. W., Lim S., 2016, *ApJ*, 822, L31
 Revaz Y., Jablonka P., 2018, *ArXiv e-prints*
 Román J., Trujillo I., 2017a, *MNRAS*, 468, 703
 —, 2017b, *MNRAS*, 468, 4039
 Rong Y., Guo Q., Gao L., Liao S., Xie L., Puzia T. H., Sun S., Pan J., 2017, *MNRAS*, 470, 4231
 Sánchez-Blázquez P., Gorgas J., Cardiel N., González J. J., 2006, *A&A*, 457, 787
 Schiavon R. P., Rose J. A., Courteau S., MacArthur L. A., 2004, *ApJ*, 608, L33
 Shi D. D. et al., 2017, *ApJ*, 846, 26
 Smith R. J., Lucey J. R., Hudson M. J., Allanson S. P., Bridges T. J., Hornschemeier A. E., Marzke R. O., Miller N. A., 2009, *MNRAS*, 392, 1265
 Thomas D., Maraston C., 2003, *A&A*, 401, 429
 Thomas D., Maraston C., Bender R., Mendes de Oliveira C., 2005, *ApJ*, 621, 673
 Trujillo I., Roman J., Filho M., Sánchez Almeida J., 2017, *ApJ*, 836, 191
 van der Burg R. F. J. et al., 2017, *A&A*, 607, A79
 van der Burg R. F. J., Muzzin A., Hoekstra H., 2016, *A&A*, 590, A20
 van Dokkum P. et al., 2016, *ApJ*, 828, L6
 —, 2017, *ApJ*, 844, L11

van Dokkum P. G., Abraham R., Merritt A., Zhang J., Geha M., Conroy C., 2015a, *ApJ*, 798, L45
 van Dokkum P. G. et al., 2015b, *ApJ*, 804, L26
 Vazdekis A. et al., 2015, *MNRAS*, 449, 1177
 Vazdekis A., Koleva M., Ricciardelli E., Röck B., Falcón-Barroso J., 2016, *MNRAS*, 463, 3409
 Venhola A. et al., 2017, *A&A*, 608, A142
 Venn K. A., Irwin M., Shetrone M. D., Tout C. A., Hill V., Tolstoy E., 2004, *AJ*, 128, 1177
 Yagi M., Koda J., Komiyama Y., Yamanoi H., 2016, *ApJS*, 225, 11
 Yozin C., Bekki K., 2015, *MNRAS*, 452, 937

APPENDIX A: STELLAR POPULATION ANALYSIS

Here we present in detail the stellar populations derived from all the different index–index pairs and both full spectral fitting codes. We measure the most relevant indices in our spectral region, which are $H\beta$ and $H\beta_0$ (Cervantes & Vazdekis 2009) as age-sensitive indices, and $Fe5015$, Mgb_{5177} , $Fe5270$ and $Fe5335$ as the metallicity-sensitive ones. We also use the following combined indices $\langle Fe \rangle' = (0.72 \times Fe5270 + 0.28 \times Fe5335)$; $[Mg/Fe]' = \sqrt{Mgb \times \langle Fe \rangle'}$ and $[MgFe50] = (0.69 \times Mgb + Fe5015)/2$ (Thomas & Maraston 2003; Kuntschner et al. 2010).

For the rest of this section we use the highly age sensitive $H\beta_0$ index rather than the $H\beta$ one, as it is shown to provide more orthogonal model grids. From each pair of age–metal indices we thus derive an SSP age and metallicity, as shown in Figure A1. In the age panel (left), the shaded areas correspond to extrapolated measurements, where the indices fall outside of the model grid. Any galaxy in that area should thus be considered as very old. We show the $[Fe/H]$ metallicities from all the different Fe lines in the middle panel. For the total metallicity $[Z/H]$ (right) we use the combination of the age sensitive index with either of the combined $[MgFe]$ indices, known to be insensitive to α -enhancements. Overall Figure A1 shows that the SSP ages derived with the different sets of indices are very robust. However, it is more difficult to obtain robust values for $[Fe/H]$ and $[Z/H]$ as the lines are in many cases affected by noise in the spectra or are near the edge of the spectra (in particular for $Fe5335$ and thus the combined $\langle Fe \rangle'$).

We then obtain the $[Mg/Fe]$ ratios using the same approach as in Vazdekis et al. (2015). We use the metallicity estimates Z_{Mgb} and Z_{Fe5015} obtained previously and the proxy $[Z_{Mg}/Z_{Fe5015}] = Z_{Mgb} - Z_{Fe5015}$. Then, using the empirical relation of Vazdekis et al. (2016) we transform it, using $[Mg/Fe] = 0.59 \times [Z_{Mg}/Z_{Fe5015}]$.

We finally perform the full spectral fitting approach to obtain mean luminosity- and mass-weighted stellar population properties. In addition, we recover the SFH of each galaxy, which is the amount of stellar mass that is created at a given time. We use both **STARLIGHT** (Cid Fernandes et al. 2005) and **STECKMAP** (Ocvirk et al. 2006) for this analysis. We remind the reader that **STECKMAP** allows the use of non-flux calibrated spectra, whereas **STARLIGHT** demands a relative-flux calibration (which contributes to a smaller sample of usable UDGs, i.e. we omit Yagi 392 and Yagi 398).

In Figure A2 we show a comparison of age and total metallicity derived from full spectral fitting with those

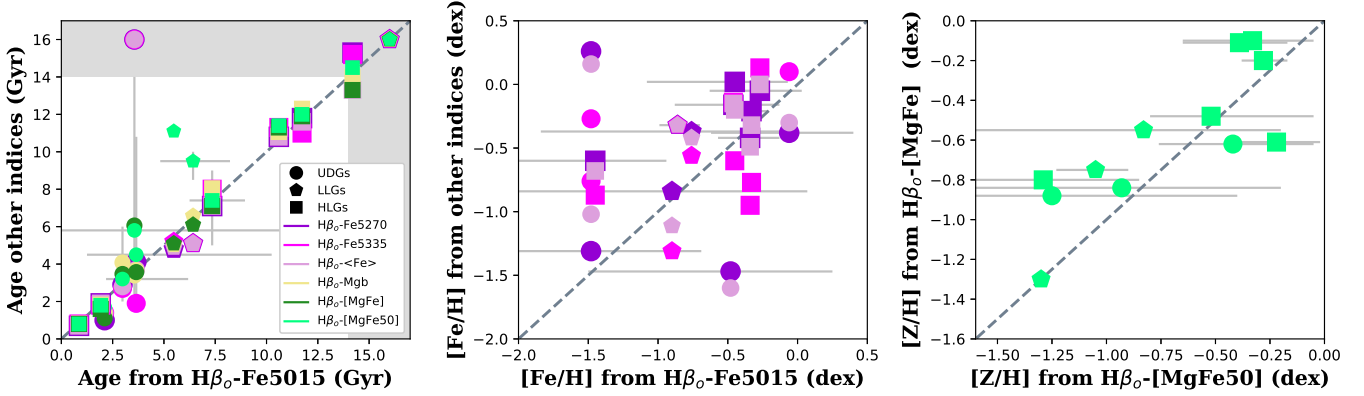


Figure 1. Line index results. We show the resulting age, [Fe/H] and total metallicity [Z/H] from different pairs of indices, using the age sensitive H β_0 for all the galaxies in the mask with enough S/N. Shaded areas in the age panel correspond to extrapolated measurements, where the indices fall outside of the model grid. The derived ages are very robust across the different indices, but larger differences are found in the metallicity panels, due to some poor line measurements.

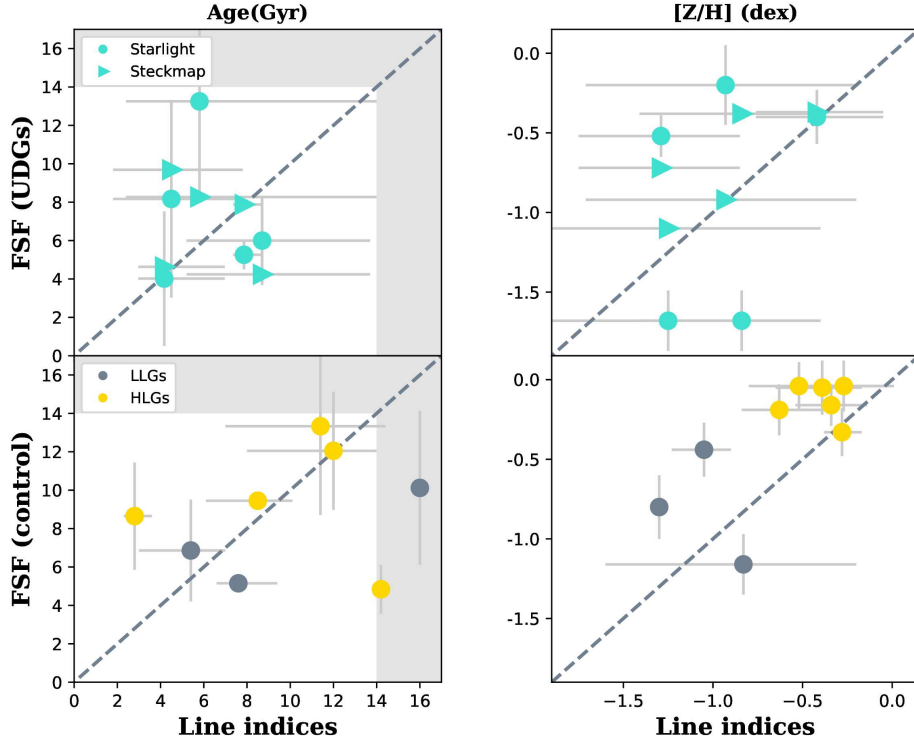


Figure 2. Comparison of the methodologies. We show the comparison between the results obtained by using the full spectral fitting approach (FSF) and those from the line indices. *Top* panels show the age (*left*) and the total metallicity (*right*) for the Coma UDGs. *Bottom* panels show the same properties derived with STARLIGHT for the control galaxies in our study, i.e Coma cluster HLG and dwarfs. Shaded areas in the age panel correspond to extrapolated measurements, where the indices fall outside of the model grid.

from line indices for Coma UDGs (top) and HLG plus dwarf galaxies (bottom). This figure shows that the ages are in general well constrained across the different methods. In some cases, larger differences are seen but they can be understood when carefully inspecting the spectra (e.g. H β lines not well fitted). The variations in the total metallicity are slightly larger, but they are all compatible with having low metallicities. Having potentially three different stellar population results to hand, we choose for the analysis those values that

we consider to be most robust, i.e. taking into account issues with crucial line indices or issues with a bad flux calibration. The final values are those used throughout Section 4 and are quoted in Table 2.

This paper has been typeset from a T \tiny E X/L \tiny A T \tiny E X file prepared by the author.